Sedimentology (1992) **39**, 143–160

Early diagenetic recrystallization of Holocene (< 3000 years old) peritidal dolomites, Ambergris Cay, Belize

JAY M. GREGG*, SCOTT A. HOWARD†[1] *and* S. J. MAZZULLO‡

*Departments of *Geology and Geophysics, and †Ceramic Engineering, University of Missouri-Rolla, Rolla, MO 65401, USA*

‡Department of Geology, Wichita State University, Wichita, KS 67208, USA

ABSTRACT

Three peritidal carbonate crusts and associated intercrust sediments (total thickness of ~30 cm; aged < 3000 years BP) on Ambergris Cay, Belize, contain 32–100% calcian dolomite ($\bar{x}$ = 72·5% dolomite) ranging in composition from 40 to 46 mol% $MgCO_3$ ($\bar{x}$ = 43·3). Dolomite replaced high Mg calcite foraminiferal muds penecontemporaneously with sedimentation, forming partially dolomitized sediments and lithified crusts. Dolomitization probably occurred in normal to moderately evaporated seawater and is apparently continuing at the present.

Detailed scanning electron microscope analysis shows a linear increase in mean dolomite crystal size with depth; 0·4 μm near the top of the section to 1·0 μm near the base of the dolomitized section. This size increase is not accompanied by any significant decrease in porosity. Crystal size distributions appear to be log-normal and become increasingly broad and flat with depth. Rietveld X-ray pattern-fitting structure refinements indicate increasing Ca and Mg concentrations on their respective sites (cation ordering) as a function of increasing depth. Most of the ordering occurs within the first 15 cm of the surface. Stoichiometry does not increase with depth indicating no relationship between the Ca/Mg ratio and cation ordering. Strong geochemical trends were observed down-section in the dolomite, including: (1) increasing Mn content (44 to 274 ppm), and (2) decreasing $\delta^{13}C$ values (−0·9 to −5·5‰ PDB). Oxygen isotope values range from $\delta^{18}O$ = 1·3‰ PDB in the upper part of the section to 2·6‰ PDB in the lower part of the section and are interpreted to represent two distinct groups of values rather than a continuous trend.

Down-section dolomite crystal size increase and shapes of crystal size distributions are consistent with recrystallization via a surface energy-driven dissolution-reprecipitation process (Ostwald ripening). The observed trends in carbon isotopes and Mn content probably result from geochemical re-equilibration during recrystallization and reflect reducing conditions and an isotopically light, organically derived, carbon source. Oxygen isotope compositions probably reflect relict original dolomite values and are a result of decreasing evaporation due to rising sea level.

INTRODUCTION

Neomorphic recrystallization has long been recognized as an important diagenetic process affecting carbonate rocks (Folk, 1965; Bathurst, 1975). Recent work on the subject has focused on the importance of neomorphic recrystallization during diagenesis of ancient dolomites (e.g. Fairchild, 1983; Gregg & Sibley, 1984; Zenger & Dunham, 1988; Fairchild *et al.*, 1989; Fairchild & Spiro, 1990; Carter & Dworkin, 1990; Gregg & Shelton, 1990; Kaufman *et al.*, 1991; Kupecz *et al.*, 1992; Mazzullo, 1992; Sibley *et al.*, 1992). Land *et al.* (1975) and Land (1980) recognized that such processes, involving fluids other than those in which the dolomite initially precipitated, commonly will significantly alter the original trace element and isotope geochemistry of the rock.

Holocene dolomites are generally characterized by submicrometre to decimicrometre crystal sizes, poor cation ordering and high Ca/Mg ratios (e.g. Illing *et al.*, 1965; Shinn *et al.*, 1965; Gebelein *et al.*, 1980; McKenzie, 1981; Carballo *et al.*, 1987; Gunatilaka *et al.*, 1987; Mazzullo *et al.*, 1987; and many others). Although it is recognized that poorly ordered and non-

[1]Present address: Rt. 2 Box 555, Rolla, MO 65401, USA.

stoichiometric dolomite is thermodynamically unstable and therefore susceptible to recrystallization, there is relatively little detailed documentation of such recrystallization occurring in Holocene dolomites. McKenzie (1981), for example, observed increasing cation ordering, stoichiometry and crystal size in Holocene dolomite in a landward traverse across a Persian Gulf coastal sabkha. She interpreted these changes to indicate crystal growth and increasing ordering and stoichiometry with ageing. Similarly, small (0·1–0·3 μm), rounded, poorly ordered, calcian dolomite crystals were observed in Holocene supratidal crusts on Sugarloaf Key, Florida, by Carballo *et al.* (1987). In contrast, older Holocene dolomitized crusts were found to contain larger (1–5 μm), euhedral dolomite rhombs which are more ordered and stoichiometric than the dolomite in the younger crusts. These larger dolomite crystals were interpreted by Carballo *et al.* (1987) to be recrystallization products of presumed pre-existing submicrometre crystals such as still exist in the younger crusts.

This paper documents early diagenetic recrystallization of Holocene peritidal dolomite on the island of Ambergris Cay, Belize. The specific term 'recrystallization' will be used here rather than the general term 'neomorphism' because there appears to be no obvious mineralogical change in the samples examined. Recrystallization here has resulted in an increase in crystal size and cation ordering, and significant changes in trace element and stable isotope geochemistry of the dolomite. It is hypothesized that this dolomite recrystallization is surface energy driven, and is thus termed Ostwald ripening (Baronnet, 1982; Morse & Casey, 1988).

Geological setting

Holocene dolomites less than 3000 years old occur on many humid-zone supratidal flats (savannahs) on Ambergris Cay in northern Belize (Fig. 1; Ebanks, 1975; Mazzullo *et al.*, 1987; Mazzullo & Reid, 1988). Regional distribution and preliminary data on the geochemistry and origin of these dolomites were discussed by Mazzullo *et al.* (1987). The most notable occurrence of dolomite is on Tomas Savannah, a low lying peritidal flat complex on south-central Ambergris Cay (Figs 1 & 2). As much as 1 m of Holocene dolomite is forming within micritic and sandy carbonate sediments composed dominantly of high Mg calcite (HMC) and subordinate aragonite (<1%) and low Mg calcite (LMC) (usually <5%). Dolomite occurs variously within single surficial crusts, mostly

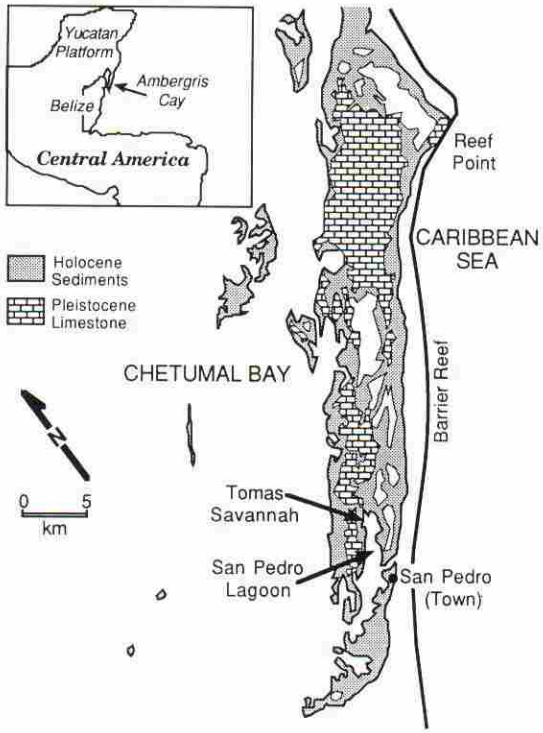

Fig. 1. Map of Ambergris Cay showing the Pleistocene and Holocene outcrops and location of the dolomitized peritidal flat (Tomas Savannah) described here.

as three separate crusts (each of which is 2–10 cm thick), locally as a single crust up to about 40 cm thick, and in weakly consolidated intercrust sediments (Fig. 2). In ascending order the three crusts have been radiocarbon dated at 2925 years, 1690 years and 905–1075 years BP. Superposition of the three crusts was interpreted to reflect dolomite formation at the air–water interface during progressive stands of rising sea level over the last 3000 years (Mazzullo *et al.*, 1987).

The dolomite is finely crystalline (generally <2·5 μm), calcic and poorly ordered. It has readily replaced HMC micrite and various foraminifera, and also occurs as intra- and interparticle cements in the crusts (Mazzullo *et al.*, 1987). Associated minor aragonitic and rare LMC allochems are not dolomitized. In fact, these allochems typically are either removed by dissolution, or the aragonite is calcitized during dolomitization (Mazzullo & Reid, 1988). In some areas, the dominantly HMC sediments directly overlying the Pleistocene limestone have been converted to LMC.

The climate on Ambergris Cay is one of seasonally varying amounts of rainfall and rates of evaporation

such that during dry seasons, the salinity of interstitial and standing water on the flats ranges from 40 to 75‰. During rainy seasons, fluid salinities on and interstitially within the flats range from 9 to 30‰, and upward discharge of meteoric fluids out of the subjacent Pleistocene limestone into the overlying basal sediments on the flats has been documented (Mazzullo *et al.*, 1987). Such meteoric influence probably accounts for the dissolution of aragonite and presence of diagenetic LMC in the sediment immediately above the Pleistocene limestone. Carbonate alkalinity of the interstitial fluids is uniformly about four times greater than that of adjoining lagoonal waters, and molar Mg/Ca ratios of lagoonal and interstitial waters on the flat average about 4:1 throughout the year (Mazzullo *et al.*, 1987). Despite the obvious schizohalinity of this environment, on the basis of the oxygen isotope composition ($\delta^{18}O$ values of the dolomite ranging from 1·2 to 2·2‰ PDB) Mazzullo *et al.* (1987) concluded that the dolomite formed from water of near normal marine composition. Dolomitization, including that affecting intercrust and the young surficial sediments, is probably continuing today (Mazzullo *et al.*, 1987).

METHODOLOGY

Dolomite was collected from Tomas Savannah by excavating sections of Holocene sediments down to the top of the Pleistocene at the four localities shown on Fig. 2. Samples of undolomitized foraminiferal sediments were collected from the lagoon and beach adjoining Tomas Savannah (Fig. 2). Individual samples were taken from the sections at approximately 2·5 cm intervals for detailed analysis. Polished thin sections were made of the dolomites for visible light microscopy, scanning electron microscopy (SEM) and electron microprobe analysis. SEM examinations were made using a JEOL JSM-T330A instrument equipped with a back-scattered electron detector. Dolomite crystal sizes were determined by measuring long diameters of crystals along linear traverses on SEM micrographs. Intercrystalline microporosity was estimated by computer automated image analysis of SEM images. Several analyses for Ca, Mg, Fe and Mn in dolomite were made using a JEOL 733 electron microprobe.

Dolomite samples prepared for isotopic and chemical analysis were hand ground to a fine powder, cleaned with 10% acetic acid and a distilled water rinse to remove $CaCO_3$, filtered, and then dried at room temperature. Samples cleaned in this way were analysed by X-ray diffraction (XRD) to assure that all $CaCO_3$ was removed. Samples analysed for isotope compositions of $CaCO_3$ (calcite and aragonite) were washed with distilled water. $CaCO_3$ isotope compositions in mixed $CaCO_3$–dolomite samples were determined from

$$\delta_{cal} = \frac{[\delta_{bulk} - (\delta_{dolo} \times \chi_{dolo})]}{\chi_{cal}},$$

where δ is the $\delta^{18}O$ or $\delta^{13}C$ value and χ_{cal} and χ_{dolo} are the atomic fractions of $CaCO_3$ and $CaMg(CO_3)_2$ in the bulk sample respectively. Stable carbon and oxygen isotope analyses were performed at the University of Michigan Stable Isotope Laboratory and at the Texaco E&P Technology Division Stable Isotope Laboratory. Calcites and dolomites were reacted with phosphoric acid at 50°C (Michigan) and 90°C (Texaco). Isotope compositions were corrected for differences in phosphoric acid reaction temperatures (Craig, 1957). No corrections were made for differences in acid fractionation between dolomite and calcite.

Samples of prepared dolomite (50–100 mg) were reacted with 5 ml of concentrated HCl and diluted to 50 ml. Dilute solutions were analysed for Fe, Mn and Sr using a Perkin-Elmer 2100 atomic absorption spectrophotometer (AA). Analyses were compared with sets of laboratory-prepared standards. Selected, similarly prepared samples were also analysed for Ca, Mg, Fe, Mn, Sr and Na using induced coupled plasma spectroscopy (ICP) at the University of Missouri Environmental Trace Substances Laboratory.

XRD analyses of powdered carbonates were made with a Philips X-ray diffractometer using Cu K_α radiation. Stoichiometry of carbonates was determined by measuring the [104] peak shift (Lumsden & Chimahusky, 1980). The dolomite content (wt%) was determined by measuring the area under the [113] reflection and comparing it to that under the [111] reflection of a weighed internal fluorite standard. The ratios obtained were compared to a set of standards prepared from fluorite and mixtures of pure calcite and dolomite (collected on Ambergris Cay). The [113] rather than the [104] dolomite reflection was used for this purpose in order to avoid error due to variability in dolomite stoichiometry (Lumsden, 1979).

Selected specimens from all three crusts were also analysed using the X-ray Rietveld structure refinement technique (Rietveld, 1969; for additional references on X-ray profile fitting methods see Howard & Preston, 1989; Post & Bish, 1989). Patterns were collected from

specimens using a Scintag PAD X-ray diffractometer using Cu K_α radiation. The data were collected in the angular range of 20–140° 2θ using a 0·02° step increment and a 2 s count time.

The structures input to the Rietveld program included both calcite and dolomite since omission of calcite would have influenced the refined structural parameters of the dolomite. Stoichiometry of calcite used in the refinement reflected the ideal $CaCO_3$ composition. A Pearson VII profile shape function was used to model the line shapes with only the V and W broadening coefficients used since the lines were so broad; refinement of the U parameter resulted in abnormally narrow lines at low angle. For details of the derivation and mathematics of these broadening coefficients see Rietveld (1969), Howard & Preston (1989) and Post & Bish (1989). Anisotropic thermal parameters and both the Ca and Mg site occupancies were varied during the refinement. Background was modelled using a 4th order polynomial function and a parameter was refined in order to accommodate specimen displacement errors.

RESULTS

Distribution and petrography of dolomite

XRD analysis of Holocene deposits from the four sections examined indicates that the three dolomite crusts and intercrust sediments contain from 32 to >99% ($\bar{x}$=72%) dolomite (Fig. 2, Table 1). Detailed SEM analyses were made on samples from the BZF 31 section (Fig. 2). All dolomite crystals examined from this section have well developed rhombic morphology and range in size from ~0·1 μm in the upper crust to >2 μm in the lower crust (Fig. 3a–c). Dolomite crystals replacing foraminifera are slightly larger. Many dolomitized foraminifera have sweeping extinction under crossed polarized light indicating mimetic replacement of HMC foraminifera. This is verified by SEM analysis which shows apparent preferred c-axis orientation of dolomite crystals replacing foraminifera (Fig. 3d,e). Rounded edges of calcite fragments adjacent to dolomite crystals with sharp edges are consistent with calcite undergoing dissolution during dolomite crystal growth (Fig. 3f).

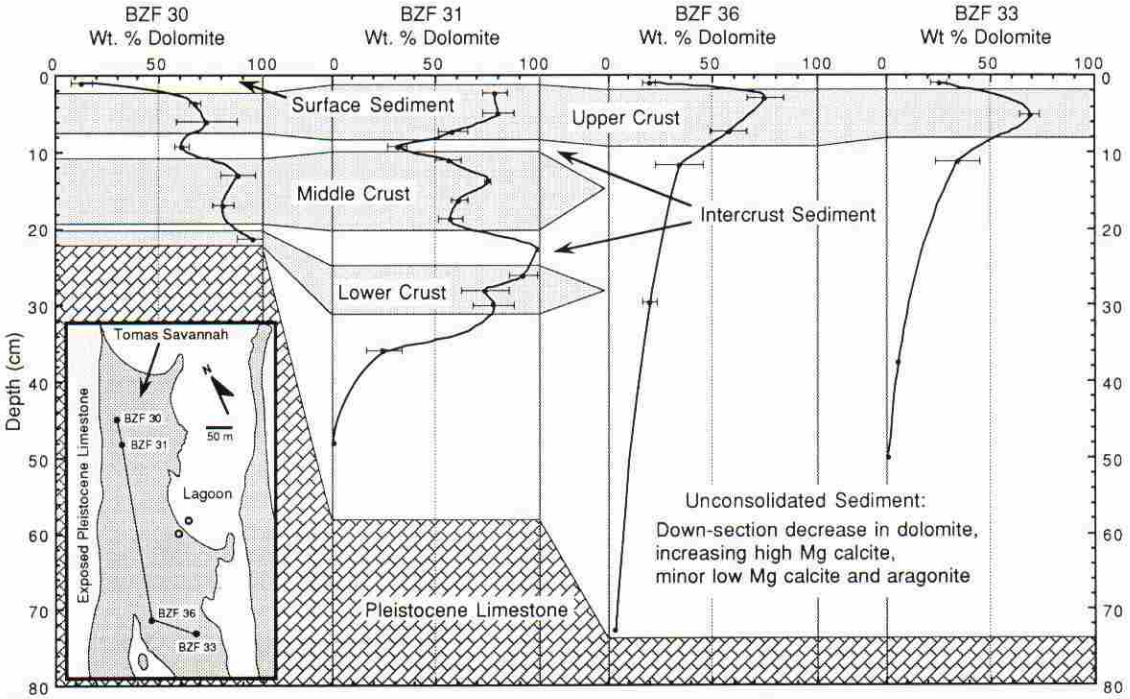

Fig. 2. Diagrammatic section through Holocene sediments and lithified crusts on Tomas Savannah (no horizontal scale is intended). The dolomite content and 95% confidence intervals were obtained from X-ray diffraction analyses (Table 1) in sediments and crusts. Inset map shows the locations of sections sampled on Tomas Savannah (closed circles) and modern lagoon and beach sediments (open circles).

Table 1. X-ray and geochemical data.

Section and sample	Depth (cm)	Dolomite (wt%)*	$MgCO_3$ (mol%)*	Fe (wt%)	Mn (ppm)	Sr (ppm)	Na (ppm)
Surface sediment							
BZF 29 1	~1·3	13·5±5·0	43·2±1·0				
Upper crust							
BZF 30 E–1	3·8	67·9±2·7	46·0±0·7	0·178†	43·9†	605·5†	1824†
BZF 30 E–2	6·4	73·7±14·4	42·9±0·5	0·245†	63·9†	463·1†	1273†
Intercrust sediment							
BZF 30 E–3	9·5	61·8±3·7	42·7±0·4	0·188†	98·4†	689·0†	1485†
Middle crust							
BZF 30 E–4	13·3	88·5±8·2	42·9±0·5	0·294†	122·4†	411·3†	1247†
BZF 30 E–5	17·2	81·6±5·2	42·7±0·1	0·243†	101·1†	514·6†	1272†
Lower crust							
BZF 30 E–6	21·6	96·1±7·9	42·7±0·3	0·303†	176·4†	400·2†	1183†
Upper crust							
BZF 31 A–2	2·5	78·9±5·8	44·6±0·6	0·436	67·7	126·1	
						462·7†	1501†
BZF 31 A–3	5·1	80·6±7·6	43·0±0·1	0·202	57·4	489·7	
BZF 31 A–4	7·6	59·0±7·0	42·6±0·4	0·369	113·1	394·4	
Intercrust sediment							
BZF 31 B–5	9·5	32·4±4·8	42·1±0·3	0·547	128·2	265·8	
Middle crust							
BZF 31 C–6	11·4	56·8±6·4	42·2±0·7	0·442	103·6	362·0	
BZF 31 C–7	14·0	75·7±1·6	42·6±0·9	0·473†	107·7†	382·6†	1170†
				0·471	114·8	435·0	
BZF 31 C–8	16·5	62·2±3·7	42·4±0·3	0·896	167·5	250·6	
BZF 31 C–9	19·0	57·8±5·6	42·1±0·8	1·026	172·3	405·3	
Intercrust sediment							
BZF 31 D–10	22·9	99·4±0·6	43·2±0·1	0·454	203·9	468·1	
				0·548†	210·9†	386·3†	1226†
Lower crust							
BZF 31 E–11	26·4	92·8±6·6	43·1±0·4	0·450	179·3	418·0	
BZF 31 E–12	28·3	74·2±11·5	42·2±0·4	0·498	218·5	502·7	
				0·357†	273·7†	585·4†	1382†
BZF 31 E–13	30·2	78·5±9·7	41·9±0·4	0·482	212·6	422·0	
Sediment							
BZF 31 F–14	36·3	25·7±8·7	42·1±0·6				
Surface sediment							
BZF 33 A–1	~1·3	26·4±4·0	42·8±1·0				
Upper crust							
BZF 33 B–2	5·4	69·8±4·8	43·7±1·3				
Sediment							
BZF 33 C–3	11·7	34·8±10·7	40·4±1·0				
BZF 33 C–4	~38	<10	40·2				
Surface sediment							
BZF 36 A–1	~1·3	20·1±3·1	42·4±0·8				
Upper crust (?)							
BZF 36 B–2	3·2	75·6±8·7	45·8±0·9				
BZF 36 B–3	7·6	58·4±8·7	42·2±0·1				
Sediment							
BZF 36 C–4	~12	34·8±11·5	41·4±0·4				
BZF 36 D–5	~30	20·6±3·8	42·0±0·4				
BZF 36 E–6	~73	<< 10	41·1				

*Analysis by X-ray diffraction (see Methodology), 3–6 replicate runs on each sample. Error was calculated using *t* distribution at 95% confidence.

† Analysis by ICP; all other elemental analyses by AA (Fe & Mn using flame, Sr using graphite furnace).

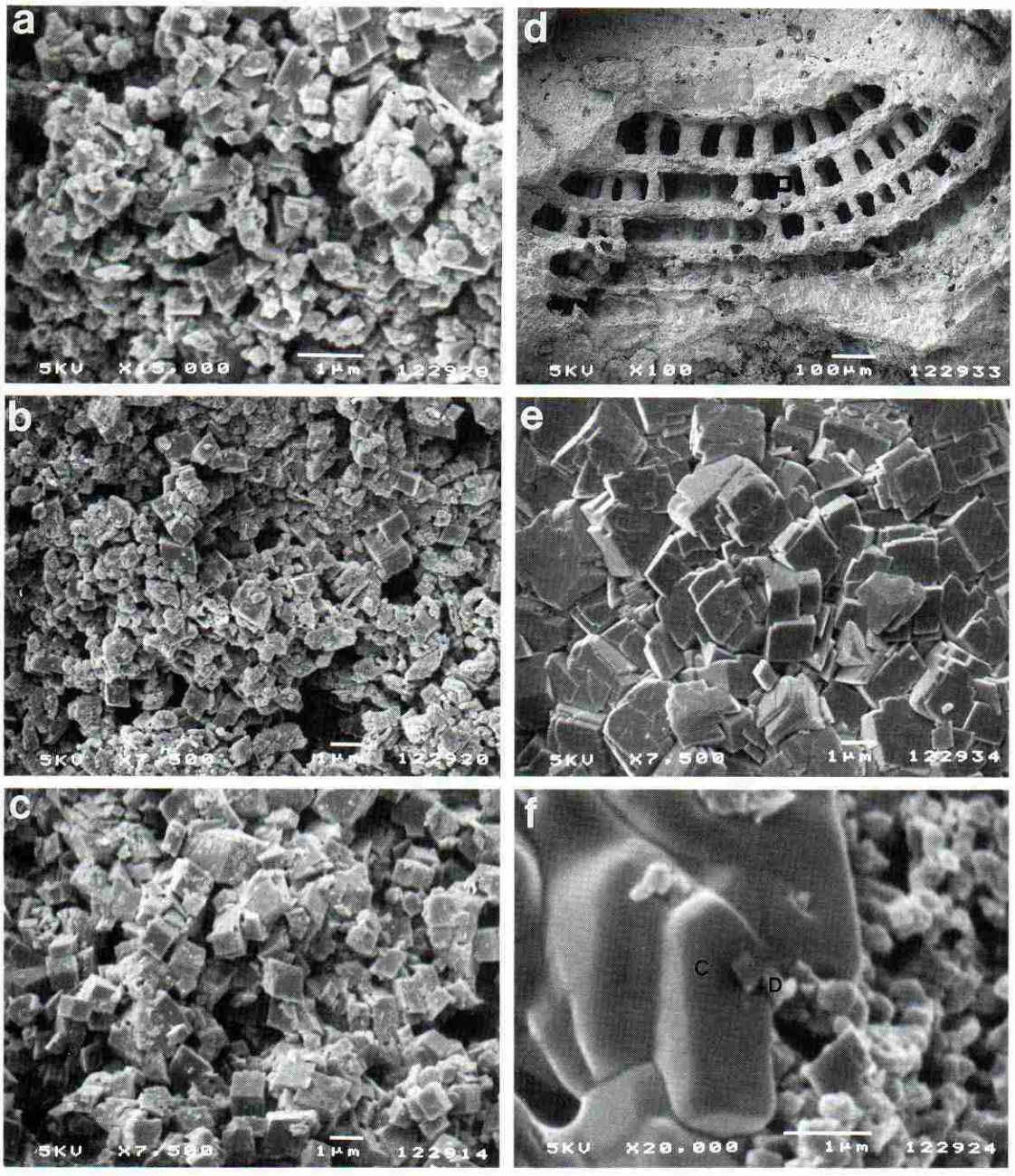

Fig. 3. SEM photomicrographs of dolomitized sediments from the BZF 31 section. (a) Dolomitized mud from the upper crust. (b) Dolomitized mud from the middle crust. (c) Dolomitized mud from the lower crust. (d) Dolomitized soritid foraminifera. (e) Detail of the outlined area of the soritid foraminifera in (d) showing *c*-axis orientation of dolomite crystals in a replaced wall. (f) Dolomite crystals (D) replacing calcite (C); note evidence of calcite dissolution (rounded corners).

The dolomite content shows a rough (but not statistically significant) down-section increase to the base of the lower crust in BZF 30. In contrast, in the unconsolidated sediment below the oldest crust the dolomite content decreases down-section in all four sections sampled (Fig. 2, Table 1). The LMC content increases in unconsolidated sediment immediately above the Pleistocene limestone. In the BZF 31 section LMC is the dominant $CaCO_3$ constituent in the lower 2 cm of the lower crust and in the underlying sediment (Table 1).

Crystal size distributions in the BZF 31 section were determined only for dolomite replacing carbonate mud to assure uniformity in size comparisons. Attempts to study size distributions for crystals replacing skeletal material (i.e. foraminifera) were unsuccessful. This was because there is too much variation between the distribution of possible nucleation sites on skeletal allochems (depending on the organism and pre-dolomitization diagenesis) to make such analysis meaningful. Initial crystal size is controlled largely by the distribution of nucleation sites on the material undergoing dolomitization (Sibley & Gregg, 1987) so comparisons must be made between materials with similar initial nucleation site distributions. There is no reason to believe that the density of nucleation sites in HMC mud would change depending on the stratigraphic position in the Holocene section or that such a change would be systematic.

The mean dolomite crystal size shows a linear increase, down-section, from ~0·4 μm in the upper crust to ~1·0 μm in the lower crust (Fig. 4). This increase, which represents more than a doubling of the mean size, is accompanied by a decrease in the number of crystals per unit volume (Fig. 3a–c) and is not accompanied by any significant decrease in porosity (see discussion below). Crystal size distributions are coarsely skewed and appear to be log-normal, becoming increasingly broad and flattened with depth (Fig. 5).

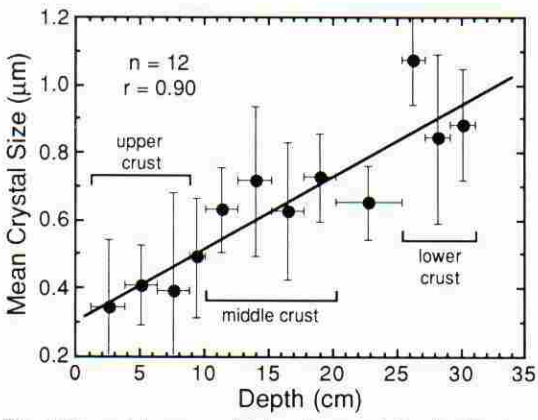

Fig. 4. Geometric means of dolomite crystal size distributions vs. depth in the BZF 31 section. Horizontal error bars represent interval sampled for analysis; vertical error bars are the geometric variances of the distributions. Locations of samples relative to dolomitized crusts are shown.

Total porosities, obtained by mercury porosimetry, range from about 40–52% in the upper and middle dolomite crust to about 30% in the lower dolomite crust (Mazzullo & Reid, 1988). Intercrystalline microporosity in dolomitized muds ranges from 22·7 to 24%, averaging 23·5%. No trend was observed between intercrystalline microporosity and depth. The variation in porosity values between SEM analysis and mercury porosimetry represents the large volume of vug, mould, interparticle and intraparticle porosity existing in these sediments which is not measurable using SEM.

Geochemistry

Stoichiometry and cation ordering

XRD analyses indicate that the dolomite is non-stoichiometric, with $MgCO_3$ compositions ranging from 40 to 46 mol% ($\bar{x}$ = 43 mol%). These values are comparable to those reported earlier by Mazzullo *et al.* (1987). No relationship was observed between increasing stoichiometry and depth. The position of highest $MgCO_3$ compositions were observed within the top 3 cm of the upper crust in the BZF 30, 31 and 36 sections (Table 1). The range of values obtained by XRD were verified with five electron microprobe analyses which had a mean value of 43·8 mol% $MgCO_3$. Compositions of HMC in the Holocene section range from 13 to 19 mol% $MgCO_3$ ($\bar{x}$ = 15 mol%). One sample, BZF 31 E–13, contains 7 mol% $MgCO_3$ with a significant component of LMC. The underlying Pleistocene limestone is composed entirely of LMC.

Figure 6 illustrates the results of using the Rietveld program to fit the measured X-ray pattern of a sample from the middle crust of the BZF 31 section. In general, the quality of fits to the calcite lines were better than those obtained for the dolomite lines when calcite and dolomite were present in approximately the same proportions. Problems with the fit to both the dolomite and calcite reflections are attributed to a markedly anisotropic broadening of the lines (reflections). SEM analysis shows that the crystallites in the specimens are well formed and distinct from one another (Fig. 3). Because the dolomite crystallites are

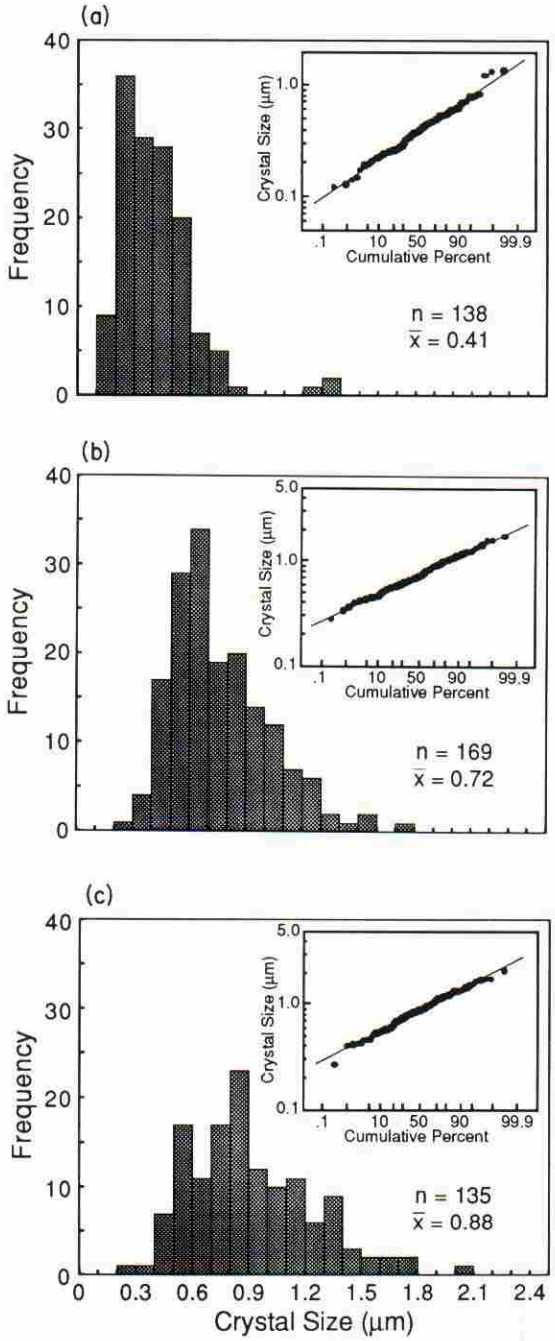

Fig. 5. Representative examples of dolomite crystal size distributions plotted as histograms and probability plots (insets). Note that the size distributions become increasingly broad and flattened with depth. The probability plots show that crystal size distributions are nearly log-normal. The examples are from the BZF 31 section: (a) upper crust, (b) middle crust, (c) lower crust.

all in the 1 μm range, line profiles should be broadened due to size effects. A variation of the crystal dimensions along different directions would be expected to broaden lines in such a way that some would appear proportionally broader than others (anisotropic broadening). Alternatively, anisotropic line broadening may be due to lattice defects such as modulation (e.g. periodic enrichment of Ca on Mg layers), heterogeneous microstructure (e.g. Reeder, 1981), or rotational disordering of the carbonate groups (e.g. Bischoff *et al.*, 1985).

A comparison of several of the refined and measured patterns shows a set of lines, in the proximity of the refined calcite lines, which are attributed to the presence of diagenetic LMC (Fig. 6). The concentration of this LMC is, in a few cases, sufficient to influence the results of the calcite structure refinements. However, any LMC lines overlapping the dolomite lines are deemed to be sufficiently small as to be inconsequential in refinement of the dolomite structure.

Site occupancies of the cations in dolomite are among the parameters refined by Rietveld analysis. Fractional site occupancies for the Ca ions on the Ca site in the dolomite unit cell are shown in Fig. 7. The concentration of Ca increases systematically as a function of depth. This trend is most pronounced in the upper 15 cm of the section and the values appear to approach 1 asymptotically (perfect ordering) with increasing depth. An inverse trend was observed for Mg on the Mg site, although it is not as strong as that found for Ca on the Ca site.

Trace elements

Trace element compositions of the dolomite, obtained from AA and ICP analyses of samples from the BZF 30 and 31 sections, are shown in Fig. 8 and Table 1. There is a strong, linear down-section increase in the Mn composition of the dolomite, from 44 to 274 ppm (Fig. 8a). Similar values and a similar down-section increase in Mn were observed in dolomite from the BZF 31 section by Lumsden & Lloyd (1988), using electron spin resonance data, indicating that the Mn is held in the dolomite crystal lattice.

The Fe content ranges from 0·18 to 1·03 wt% ($\bar{x}$ = 0·43 wt%), with a relatively weak (statistically significant at a 90% confidence level) down-section increase (Fig. 8b). Five electron microprobe analyses give an average Fe level in the dolomite of < 0·2 wt%. Variation in Fe compositions observed with AA and ICP from those observed with the microprobe may be the result of unavoidable Fe contamination from

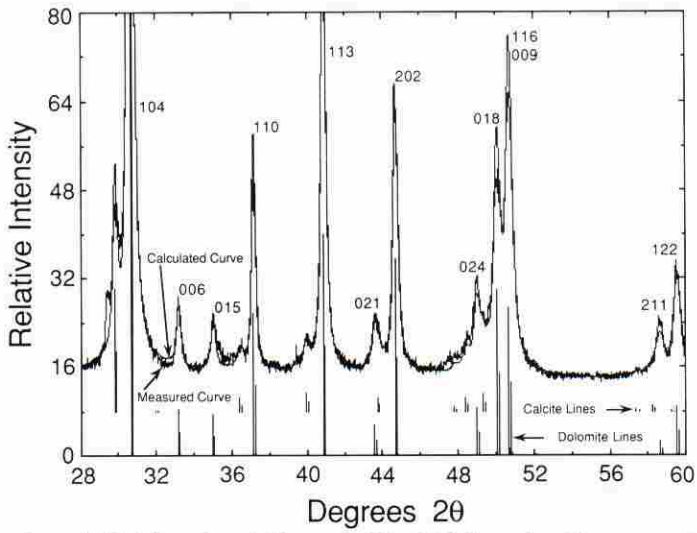

Fig. 6. X-ray diffraction of sample C–8 from the middle crust of the BZF 31 section. The measured and Rietveld calculated curves are labelled; note the close fit between the two. Positions of the high Mg calcite and dolomite lines are shown and the principal dolomite lines are labelled.

organic material or the presence of acid-soluble FeS leached from the sample during the wet chemical analyses. H_2S gas has been identified, possibly emanating from the underlying Pleistocene limestone, from the hole where the section BZF 30 was collected.

A weak (statistically significant at a 90% confidence level) down-section decrease in Na was observed; 1170–1824 ppm ($\bar{x}=1340$ ppm; Fig. 8c). The Sr composition of the dolomite ranges from 126 to 689 ppm ($\bar{x}=429$ ppm), with no apparent relationship to depth (Fig. 8d).

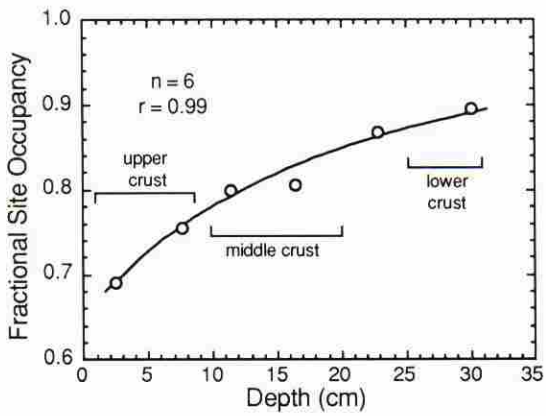

Fig. 7. Fractional site occupancy of Ca vs. depth as determined from Rietveld structure refinements on six samples from the BZF 31 section. The data are fitted to a curve with the form $y=1-a/(x+b)^2$. Locations of samples relative to dolomitized crusts are shown.

Stable isotopes

Stable isotope compositions of carbonates from Tomas Savannah are shown in Figs 9, 10 & Table 2. A down-section enrichment in $\delta^{18}O$ values (PDB) was observed for dolomite in the BZF 30 and 31 sections, from 1·33‰ in the upper crust to 2·62‰ in the lower crust. The oxygen isotope data are interpreted to represent two distinct groups or clusters of data rather than a linear trend (Fig. 9a). A very strong linear trend of decreasing $\delta^{13}C$ values was also observed, −0·90‰ in the upper crust to −5·51‰ in the lower crust (Fig. 9b). These carbon and oxygen isotope values compare favourably with those reported by Mazzullo *et al.* (1987) who also noted lower $\delta^{13}C$ values in the lower dolomite crust.

The $\delta^{18}O$ values of the dominantly HMC calcareous fraction of the Holocene sediments from the BZF 30 and 31 sections decrease with depth, from −0·13‰ in the upper crust to −1·95‰ in the lower crust. One anomalous value of 3·83‰ was observed from the uppermost 2·5 cm of the section (Fig. 10, Table 2). The $\delta^{13}C$ values of the HMC sediments also show a down-section decrease, from −0·43‰ in the upper crust to −7·85‰ in the lower crust (Fig. 10, Table 2). The lowermost value is for a calcite sample (BZF 31 E–13, Table 2) containing significantly lower $MgCO_3$ than the overlying samples (7 mol% as opposed to 15 mol% $MgCO_3$; see discussion of HMC above). This trend is similar to that observed for carbon

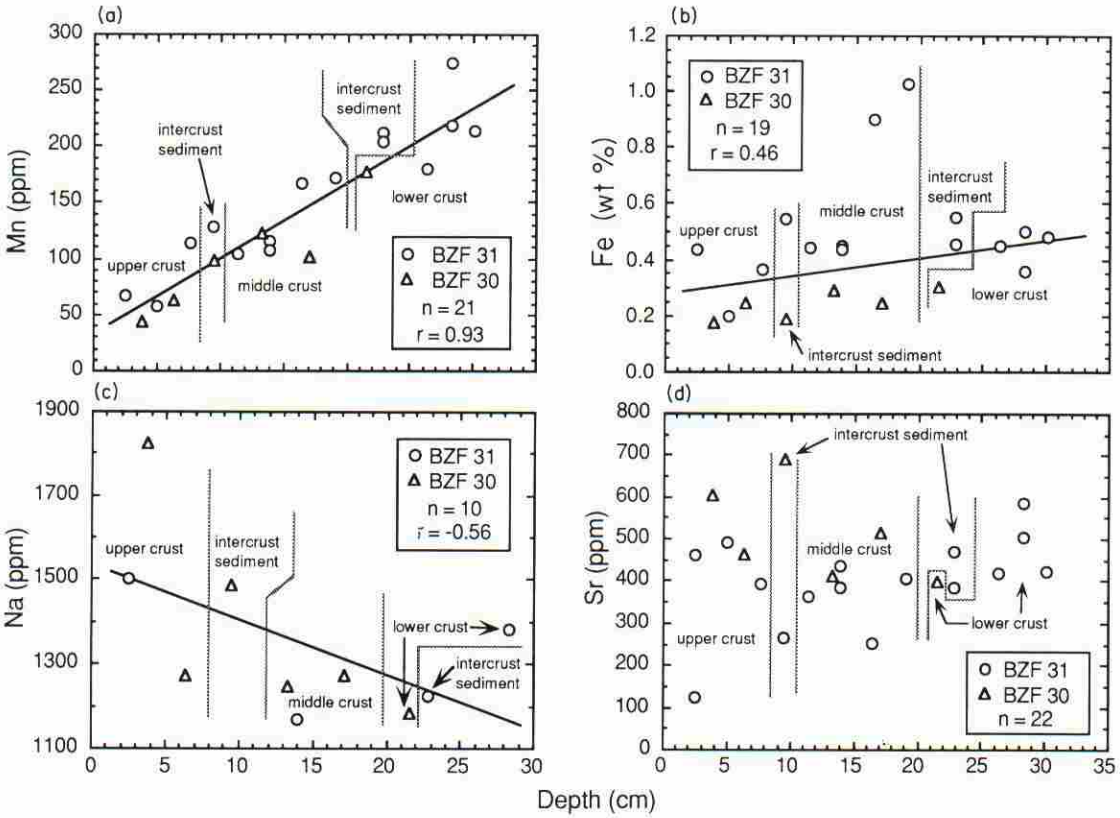

Fig. 8. Trace element composition of dolomite vs. depth from the BZF 30 and 31 sections: (a) Mn, (b) Fe, (c) Na and (d) Sr. Locations of samples relative to dolomitized crusts and intercrust sediments are shown.

isotope composition of dolomites in the same sections (Fig. 9b). Four analyses of Pleistocene limestone collected at the base of the BZF 30 and 31 sections range from $\delta^{18}O = -2{\cdot}51$ to $-1{\cdot}89‰$ and $\delta^{13}C = -7{\cdot}70$ to $-2{\cdot}56‰$. Isotope values for three samples of modern calcareous sediment composed dominantly of HMC soritid and miliolid foraminifera from the nearby beach and lagoon (Fig. 2) average $\delta^{18}O = 0{\cdot}32‰$ and $\delta^{13}C = 0{\cdot}52‰$ (Fig. 10, Table 2).

DISCUSSION

Dolomite recrystallization

Ostwald ripening: theory

Ostwald ripening (Ostwald, 1900) is the process of surface energy-driven recrystallization whereby large crystals grow at the expense of small crystals. Mathematical treatments of Ostwald ripening and resultant theoretical crystal size distributions are given by Lifshitz & Slyozov (1961) and Wagner (1961). Summaries of the process, as well as applications to various geological problems, are presented elsewhere (Baronnet, 1982; Morse & Casey, 1988; Steefel & van Cappellen, 1990). The following is a brief qualitative description of the process.

In a supersaturated solution undergoing crystal nucleation, crystallites are continuously forming. Some of these particles attain a critical radii (r^*), and are termed critical nuclei. Particles of a size $< r^*$ will dissolve back into the solution and those of a size $\geqslant r^*$ will continue to grow, forming larger crystals. The size of r^* is determined by the activation energy for nucleation, which is a function of supersaturation and the surface free energy of the nuclei (Walton, 1969). Ostwald ripening begins toward the end of the initial nucleation and growth process. Near equilibrium, r^* increases as the degree of supersaturation decreases. As r^* increases, small crystals with radii $< r^*$ will dissolve and the solute will reprecipitate on the surface of crystals with radii $\geqslant r^*$ which continue

Table 2. Stable isotope data (‰ PDB)

Section and sample	Depth (cm)	Dolomite		Calcite/aragonite	
		$\delta^{18}O$	$\delta^{13}C$	$\delta^{18}O$	$\delta^{13}C$
Upper crust					
BZF 30 E–1	3·8	1·65	−0·90	−0·28	−1·00
BZF 30 E–2	6·4	1·67	−1·92	−0·13	−1·63
Intercrust sediment					
BZF 30 E–3	9·5	1·87	−2·24	−0·60	−1·36
Middle crust					
BZF 30 E–4	13·3	2·58	−2·23		
BZF 30 E–5	17·2	2·54	−2·56	−0·05	−0·96
Lower crust					
BZF 30 E–6	21·6	2·44	−3·42		
Pleistocene limestone (LMC)					
BZF 30–A	24·1			−1·99	−7·70
BZF 30–B	39·2			−1·89	−2·56
Upper crust					
BZF 31 A–2	2·5	1·74*	−1·16*		
		1·33	−1·36	3·83	0·43
BZF 31 A–3	5·1	1·55*	−2·39*		
BZF 31 A–4	7·6	1·59*	−2·48*	−0·63*	−2·14*
Intercrust sediment					
BZF 31 B–5	9·5	1·46*	−2·88*	−0·60*	−2·45*
Middle crust					
BZF 31 C–6	11·4	1·85*	−3·27*		
BZF 31 C–7	14·0	1·98*	−3·41*		
		2·68	−2·81	−0·21	−2·39
BZF 31 C–8	16·5	2·39*	−3·87*		
BZF 31 C–9	19·0	2·42*	−3·84*		
		2·44*	−3·81*	−1·38*	−2·95*
Intercrust sediment					
BZF 31 D–10	22·9	2·61*	−4·52*		
Lower crust					
BZF 31 E–11	26·4	2·60*	−4·87*		
BZF 31 E–12	28·3	2·54*	−5·27*		
BZF 31 E–13	30·2	2·62*	−5·51*	−1·95*	−7·85*
Pleistocene limestone (LMC)					
BZF 31–G	~58			−2·51	−5·05
				−2·39	−5·04
Modern beach sediment (foraminifera and mollusc fragments; HMC, aragonite, minor LMC)					
BZF 24	0–1			0·32	0·06
Foraminifera from beach sediment (HMC, LMC)					
BZF 24	0–1			0·31	0·84
Modern foraminifera from lagoon (HMC, LMC)					
BZF 63	0–1			0·32	0·67

*Isotope analysis run at University of Michigan Stable Isotope Laboratory, remainder run at Texaco E&P Technology Division Stable Isotope Laboratory.

to grow. During this process there is no gain or loss of volume. However, the number of individual crystals per unit volume decreases and therefore there is no change in porosity. Theoretical equilibrium is reached when a final single crystal exists or all of the crystals are the same size.

Three kinetic steps are involved in Ostwald ripening: dissolution, transfer and growth. Of these, growth is usually considered rate limiting because there are generally fewer active sites for growth on a crystal face than for dissolution (Baronnet, 1982). Theoretical crystal size distributions resulting from volume diffu-

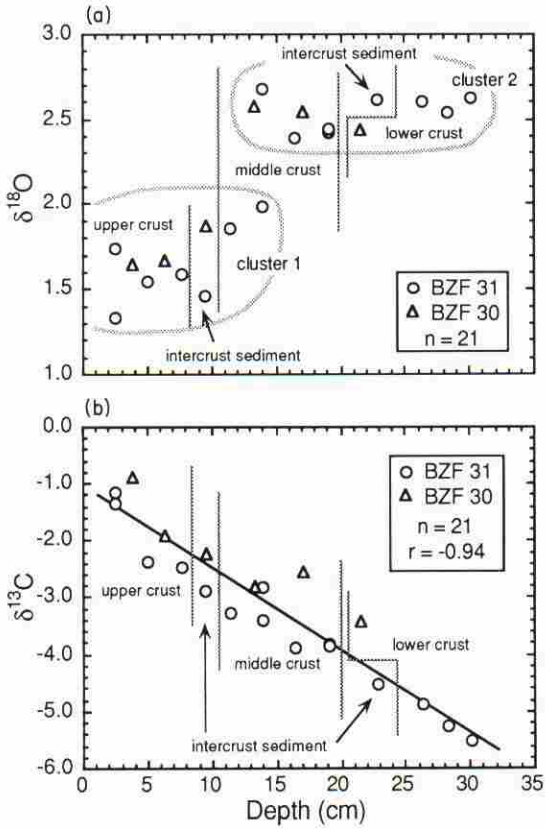

Fig. 9. Oxygen and carbon isotope compositions (‰ PDB) of dolomite from the BZF 30 and BZF 31 sections: (a) $\delta^{18}O$ vs. depth, (b) $\delta^{13}C$ vs. depth. Locations of samples relative to dolomitized crusts and intercrust sediments are shown. Two distinct clusters of oxygen isotope values are shown on (a).

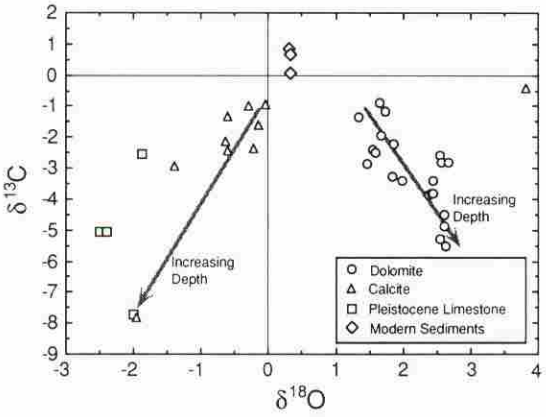

Fig. 10. Stable isotope compositions (‰ PDB) of dolomite and high Mg calcite (HMC) from crusts and intercrust sediments, Pleistocene limestone, and modern $CaCO_3$ sediments. The dolomite, HMC and Pleistocene limestone samples are from the BZF 30 and 31 sections on Tomas Savannah and the modern sediments are from the adjacent lagoon and beach (Fig. 2).

sion and first order reaction controlled crystal growth were verified experimentally by Exner & Lukas (1971). They also determined that as ripening proceeds, size distribution profiles achieve a recognizable 'stationary distribution' when plotted on reduced coordinates. Ostwald ripening of ionic crystals in aqueous solutions proceeds more slowly than the above cases and is generally thought to be controlled by second order kinetics (Hohmann & Kahlweit, 1972). This results in coarse skewed crystal size distributions as observed in some geological materials (e.g. Chai, 1974; Baronnet, 1982; Sibley *et al.*, 1992).

Theoretical treatments of Ostwald ripening assume a thermodynamically closed system (Lifshitz & Slyozov, 1961; Wagner, 1961). However, the process has been applied to many open systems in geology (Baronnet, 1982; Morse & Casey, 1988; Eberl *et al.*, 1990), including aggrading neomorphism in calcites (e.g. Lerman, 1979, p. 365, fig. 7.8). A mathematical treatment of Ostwald ripening proposed by Beenakker & Ross (1985) shows that the process in an open system is essentially equivalent to that in a closed system. For a system immersed in a fluid reservoir, diffusive interactions between the crystals undergoing ripening screen the system from the effects of the reservoir. The influence of the reservoir is therefore felt only at the boundaries of the system (Beenakker & Ross, 1985).

Application to Holocene dolomites

Ostwald ripening occurs commonly during burial diagenesis and metamorphism (Baronnet, 1982; Morse & Casey, 1988) and has been recognized as important during diagenesis of clay minerals (Eberl *et al.*, 1990; Steefel & van Cappellen, 1990; Jahren, 1991). Crystal size distributions that suggest surface energy-driven recrystallization have been observed in Precambrian detrital dolomite associated with glacial deposits (Fairchild, 1983; Fairchild *et al.*, 1989; Fairchild & Spiro, 1990). However, Ostwald ripening has not previously been verified in dolomite existing in the surficial, early diagenetic environment.

The down-section (increasing age) increase in dolomite crystal size (over a vertical distance of ~30 cm; Fig. 4) is suggestive of grain growth due to recrystallization. Additionally, progressive down-section broadening and flattening of the dolomite crystal size distributions (Fig. 5) is an important characteris-

tic feature of Ostwald ripening (Markworth, 1970; Baronnet, 1982, fig. 7; Morse & Casey, 1988). The total volume of dolomite appears not to increase significantly with increasing crystal size although the number of crystals per unit volume seems to decrease. This is verified by SEM analysis and mercury porosimetry (Mazzullo & Reid, 1988) which indicate no significant down-section decrease in porosity, especially in the dolomitized muds. Therefore, increasing dolomite crystal size is not due to syntaxial precipitation of new dolomite cement on earlier formed crystals.

Normalized crystal size distributions for representative samples of dolomite from the BZF 31 section are plotted on reduced coordinates in Fig. 11. The crystal size distribution resulting from primary nucleation and growth of the dolomite, if it differed from the observed profiles, has apparently been obliterated by recrystallization. The profiles have achieved coarse-skewed stationary distributions which are close to log-normal. The distributions also closely approximate a second order kinetics profile derived empirically for calcite which was recrystallized in laboratory hydrothermal experiments (Chai, 1974). Eberl *et al.* (1990) and Eberl (pers. comm., 1991) point out that many natural materials which have undergone Ostwald ripening will have a log-normal crystal size profile which sometimes is mistaken for a second order profile. They suggested that the log-normal distribution represents a fourth reaction mechanism which is not presently understood (the other three reaction mechanisms being volume diffusion, and first and second order kinetics). This view is supported by studies on Ostwald ripening of millimetre-sized ice crystals which were statistically shown to have log-normal size distributions (Colbeck, 1986, 1987). The data presented here appear to fit either the second order profile of Chai (1974) or a log-normal profile; however, a second order profile should truncate at $r/\bar{r} \approx 2{\cdot}25$ rather than continue to tail-off as is the case for the log-normal profile (Fig. 11).

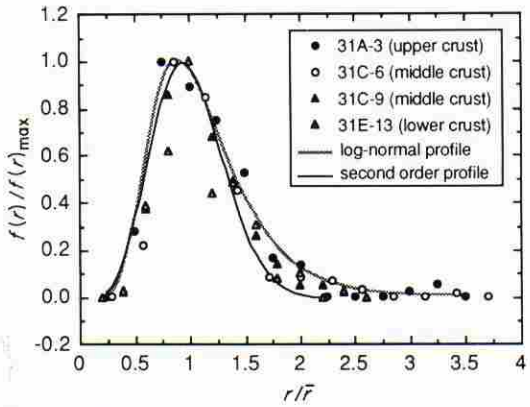

Fig. 11. Normalized crystal size distributions for representative samples from the upper, middle and lower crusts in the BZF 31 section. Parameters are: $r/\bar{r}$ = crystal size (radius) divided by mean radius and $f(r)/f(r)_{max}$ = frequency in each size category divided by the maximum frequency. The log-normal distribution curve is fitted to the normalized BZF 31A–3 data. The theoretical second order kinetics curve was calculated using the equation empirically derived by Chai (1974) for calcites recrystallized under hydrothermal conditions in the laboratory.

Stoichiometry and cation ordering

Despite recrystallization of the dolomite there does not seem to be a systematic change in dolomite stoichiometry with depth (Table 1). Dolomite compositions range between 40 and 43 mol% $MgCO_3$, with the exception of the top 2 cm of the upper crust which has a higher (44–46 mol%) $MgCO_3$ content. Dolomite forming in surficial sediments overlying the upper crust has lower $MgCO_3$ contents (averaging 42·8 mol%) which is characteristic of the rest of the section. The higher Mg content of the top 2 cm of the upper crust is possibly due to slightly different conditions (higher salinity?) during precipitation. The fact that dolomite, undergoing recrystallization, seems to remain non-stoichiometric suggests that calcian dolomite is metastable in this near surface, marine-dominated environment and that recrystallization is not stoichiometry driven.

A down-section increase in cation ordering of the dolomite was observed in the BZF 31 section (Fig. 7). This increase in ordering is most pronounced in the first 15 cm of the section (in the upper crust and half way through the middle crust) and seems asymptotically to approach perfect cation ordering with depth. These data indicate that crystal growth during Ostwald ripening may proceed more slowly than growth during initial precipitation, which may be rapid enough to inhibit ordering (Folk & Land, 1975). Slower growth would allow a higher degree of cation ordering during the recrystallization process. Cation ordering should increase the thermodynamic stability of dolomite. It is not clear what the energy contribution of ordering is to the total of the system studied here, but it is probably small as the total down-section increase in ordering is relatively small, particularly in the lower part of the section (Fig. 7).

Problems related to application of the Ostwald ripening hypothesis

Ostwald ripening requires that large dolomite crystals grow at the expense of small crystals which, in turn, undergo dissolution. Although evidence for calcite dissolution was found with SEM (Fig. 3f), such evidence for small dolomite crystal dissolution was not unambiguously observed. Rounded edges of crystals are not expected if dissolution is surface controlled (Berner, 1981, fig. 4) and etch pits on the micrometre-sized crystal surfaces are beyond the resolving power of SEM. Additionally, difficulty in observing dissolution features may be due to crystals smaller than the critical nucleus size (r^*) undergoing very rapid dissolution (Markworth, 1970) and therefore rarely being preserved.

A more serious problem with application of the Ostwald ripening hypothesis to dolomites studied here arises from the large flux of water through the Holocene section on Tomas Savannah (Mazzullo *et al.*, 1987). Although diffusive interactions between crystals tend to screen the system undergoing ripening from the bulk solution (Beenakker & Ross, 1985) and most of the fluid flux would pass through the macroporosity, large seasonal changes in solution chemistry might be expected to have a disruptive effect on the ripening process. Solubility differences in dolomite crystals due to size difference, in the size ranges reported here, are probably small. It may therefore be difficult to maintain the proper solution composition to drive Ostwald ripening, even in the screened system (J. W. Morse, pers. comm.). This problem cannot be fully resolved until better data are obtained for fluid chemistry on Tomas Savannah.

Chemical drives for recrystallization, other than Ostwald ripening, include cation ordering and increasing stoichiometry. Significant cation ordering in dolomite occurs only within the first 15 cm of the section (Fig. 7) and evidence for increasing stoichiometry with time is completely lacking. Textural evidence for Ostwald ripening is very strong and includes the increase of dolomite crystal size (Fig. 4), the shapes of the size distributions (Fig. 5), and the stationary distribution profile (Fig. 11). We favour therefore Ostwald ripening as the principal mechanism for recrystallization of dolomite on Tomas Savannah, despite the problems discussed above.

Geochemical considerations

An increase in the average crystal size by a factor of 2·5 (Fig. 4), as observed in dolomite from the BZF 31 section, results in almost 80% volume transfer of original material (Chai, 1974, fig. 8). This magnitude of volume transfer should result in chemical re-equilibration with the fluid in which recrystallization occurs (e.g. Anderson & Chai, 1974; Chai, 1975). Strong down-section trends of increasing Mn (Fig. 8a) and decreasing $\delta^{31}C$ (Fig. 9b) accompanied by a weaker trend of increasing Fe (Fig. 8b) were observed over a small (~30 cm) stratigraphic distance in dolomite from the BZF 30 and 31 sections (Fig. 2). These trends possibly resulted from recrystallization of the dolomite under reducing conditions in water containing soil-derived, $\delta^{13}C$-enriched carbon (Hudson, 1977) which moved laterally through the sediment or upward from the underlying Pleistocene limestone. This view is consistent with depleted carbon isotope values obtained for the Pleistocene limestone (Fig. 10). Negative correlations between $\delta^{13}C$ and Mn in sedimentary Mn carbonate deposits have also been attributed to manganese oxyhydroxide reduction coupled with organic matter oxidation resulting from bacterial action near the sediment–water interface (Orkita *et al.*, 1988; Polgári *et al.*, 1991).

Sodium compositions of dolomite samples from the BZF 30 and 31 sections fall within the range expected for dolomite precipitated from moderately evaporated seawater, not yet at the point of gypsum precipitation (Fritz & Katz, 1972; Sass & Bein, 1988). The weak down-section decrease in Na (Fig. 8c) may reflect a partial re-equilibration with more dilute fluids during recrystallization.

Strontium compositions fall below those observed by Behrens & Land (1972) for dolomite precipitated from seawater. However, the distribution coefficient of Sr (D^{Sr}_{dolo}) may decrease with a decreasing rate of precipitation (Kitano *et al.*, 1971; Land, 1980) which may have occurred during recrystallization. Vahrenkamp & Swart (1990), on the other hand, report a range of D^{Sr}_{dolo} estimates for dolomite precipitated from near normal marine water that are substantially lower than previous estimates. The Sr compositions for dolomite obtained in this study are slightly higher, but overlap, the range of values reported by Vahrenkamp & Swart (1990) in dolomite with stoichiometry ranging from 40 to 46 mol% $CaCO_3$. Interaction of the recrystallization fluid with underlying Pleistocene limestone may have resulted in higher Sr values.

Oxygen isotope values group into two distinct clusters (Fig. 9a): (1) samples taken largely at depths above 14 cm having a mean $\delta^{18}O$ value of 1·7‰, and (2) samples collected below 14 cm with a mean $\delta^{18}O$ value of 2·5‰. These two groups of ^{18}O data are

interpreted to represent variation in sea level stands. Sea level was lower 3000 years ago at the presumed onset of dolomitization on Tomas Savannah (Mazzullo *et al.*, 1987). Diagenesis at that time may have occurred under more evaporitic conditions than exist at present, resulting in a higher $\delta^{18}O$ value. With a rise in sea level the effects of evaporation may have decreased and the ^{18}O content of precipitating dolomite also decreased. If this view is correct, the present $\delta^{18}O$ value of the dolomite is not in equilibrium with the original water but probably represents an intermediate value between the dolomite originally precipitated and dolomite in equilibrium with water in which recrystallization took place. The influence of the recrystallization fluid on the present ^{18}O content (or, for that matter, the present $\delta^{13}C$ and trace element contents) of the dolomite is dependent on the volume transfer of original material during recrystallization (Chai, 1974). The magnitude of volume transfer increases down-section with increasing recrystallization.

Carbon and oxygen isotope values for modern lagoon and beach sediment (Fig. 10) probably are nearly in equilibrium with lagoonal water. Lower $\delta^{18}O$ values in $CaCO_3$ samples from the BZF 30 and 31 sections (Fig. 10) suggest diagenesis in dilute (mixed?) water. This contrasts with the higher $\delta^{18}O$ values obtained for coexisting dolomite. This discrepancy is explained by seasonal fluctuations in water salinity on Tomas Savannah (Mazzullo *et al.*, 1987). A scenario can be constructed where during the dry season dolomitization occurs at supersaturation in seawater modified by evaporation. Ostwald ripening probably occurs during those periods when the water composition is nearer dolomite saturation, because as supersaturation decreases, the critical nucleus size (r^*) tends to increase, driving the ripening process. During the rainy season aragonite dissolution and inversion of HMC to LMC probably occur (Mazzullo *et al.*, 1987). Within this diagenetic milieu, water moving into the Holocene section from the underlying Pleistocene limestone or basal sediments (Fig. 2) is charged with organic carbon, resulting in decreased $\delta^{13}C$ values.

Implications for ancient dolomites

Recognition of recrystallization in dolomite is important if the chemical compositions of ancient dolomites are to be interpreted correctly. Ancient dolomites commonly have very little resemblance to their modern analogues on Ambergris Cay and elsewhere in terms of crystal sizes or petrographical textures. Many ancient dolomites, precipitated under peritidal conditions, have much nearer to ideal stoichiometries than the Holocene dolomite studied here (Lumsden & Chimahusky, 1980). Further recrystallization (neomorphism) almost certainly occurs and is probably driven by non-stoichiometry (e.g. Carballo *et al.*, 1987) in addition to surface energy (Ostwald ripening). Ancient dolomite commonly is altered by basinal and sometimes magmatic fluids during burial diagenesis (e.g. Banner *et al.*, 1988; Cervato, 1990; Gregg & Shelton, 1990; Amthor & Friedman, 1991; Kupecz & Land, 1991), further altering the texture and chemical composition. The problem of multiple periods of dolomite diagenesis was recognized by Land (1980), who suggested that ancient dolomite sequences may '. . . have undergone massive chemical neomorphism' which potentially obscures the original chemical composition of the rock. This study indicates that such neomorphic recrystallization, resulting in textural change and significant changes in trace element and stable isotope composition, may begin very early during diagenesis.

CONCLUSIONS

Early diagenetic recrystallization of calcian dolomite on Tomas Savannah increased the mean crystal size from ~0·4 to ~1 μm in a down-section direction. The primary drive for recrystallization of the dolomite probably is reduction of surface free energy (Ostwald ripening). This view is supported by crystal size distributions which are coarse skewed and become more broad and flattened with increasing age (down-section). Normalized crystal size profiles fit either a second order kinetic or log-normal profile, both of which are characteristic of Ostwald ripening.

Increasing cation ordering with age is observed. However, increasing stoichiometry (Mg/Ca ratio) of the dolomite with age was not observed, indicating that cation ordering and stoichiometry are not necessarily related. This observation also indicates that recrystallization was not driven by stoichiometry.

Trace element and stable isotope geochemistry of the dolomite reflects continuous re-equilibration with pore fluids during recrystallization resulting in significant chemical change in the dolomite. Therefore, the chemical compositions of the Holocene dolomites studied here do not reflect the chemistry of the water from which they initially formed.

ACKNOWLEDGMENTS

This work was partially supported by a grant to J.M.G. from Texaco E&P Technology Division. Preliminary portions of this study, including much of the X-ray diffraction work, was completed by J.M.G. while at St Joe Minerals Corporation, Geological Research Laboratory in Viburnum. We thank R.W. Smith and P.D. Tepesch for assistance with X-ray analysis, D.R. Brosnahan for electron microprobe analyses and F.S. Miller for assisting with scanning electron microscopy. We thank K.C. Lohmann at the University of Michigan, Ann Arbor, and W.C. Dawson at Texaco E&P Technology Division, Houston, for stable carbon and oxygen isotope analyses. K.L. Shelton assisted in interpretation of stable isotope data. We thank J.E. Amthor, D.D. Eberl, J.D. Humphrey, L.S. Land, J.W. Morse and D.F. Sibley, who reviewed this manuscript during various stages of its development and editor S.D. Burley for his suggestions. The authors are responsible for any shortcomings that remain.

REFERENCES

AMTHOR, J.E. & FRIEDMAN, G.M. (1991) Dolomite-rock textures and secondary porosity development in Ellenburger Group carbonates (Lower Ordovician), west Texas and southeastern New Mexico. *Sedimentology*, **38**, 343–362.

ANDERSON, T.F. & CHAI, B.H.T. (1974) Oxygen isotope exchange between calcite and water under hydrothermal conditions. In: *Geochemical Transport and Kinetics* (Ed. by A.W. Hoffman, B.J. Gilletti, H.S. Yoder & R.A. Yund), *Carnegi Institution of Washington Publication*, **634**, 219–227.

BANNER, J.L., HANSON, G.N. & MEYERS, W.J. (1988) Water-rock interaction history of regionally extensive dolomites of the Burlington-Keokuk Formation (Mississippian): isotopic evidence. In: *Sedimentology and Geochemistry of Dolostones* (Ed. by V. Shukla & P.A. Baker), *Spec. publs Soc. econ. Paleont. Miner.*, **43**, 97–113.

BARONNET, A. (1982) Ostwald ripening in solution. The case of calcite and mica. *Estudios Geol.*, **38**, 185–198.

BATHURST, R.G.C. (1975) *Carbonate Sediments and their Diagenesis*. Elsevier, New York, 658 pp.

BEENAKKER, C.W.J. & ROSS, J. (1985) Theory of Ostwald ripening for open systems. *J. chem. Phys.*, **83**, 4710–4714.

BEHRENS, E.W. & LAND, L.S. (1972) Subtidal Holocene dolomite Baffin Bay, Texas. *J. sedim. Petrol.*, **42**, 803–811.

BERNER, R.A. (1981) Kinetics of weathering and diagenesis. In: *Kinetics of Geochemical Processes: Reviews in Mineralogy*, Vol. 8 (Ed. by A.C. Lasaga & R.J. Kirkpatrick), pp. 111–134. Mineralogical Society of America.

BISCHOFF, W.D., SHARMA, S.K. & MACKENZIE, F.T. (1985) Carbonate ion disorder in synthetic and biogenic magnesian calcites: a Raman spectral study. *Am. Miner.*, **70**, 581–589.

CARBALLO, J.D., LAND, L.S. & MISER, D.E. (1987) Holocene dolomitization of supratidal sediments by active tidal pumping, Sugarloaf Key, Florida. *J. sedim. Petrol.*, **57**, 153–165.

CARTER, K.E. & DWORKIN, S.I. (1990) Channelized fluid flow through shear zones during fluid-enhanced dynamic recrystallization, Northern Apennines, Italy. *Geology*, **18**, 720–723.

CERVATO, C. (1990) Hydrothermal dolomitization of Jurassic–Cretaceous limestones in the southern Alps (Italy): relation to tectonics and volcanism. *Geology*, **18**, 458–461.

CHAI, B.H.T. (1974) Mass transfer of calcite during hydrothermal recrystallization. *Geochemical Transport and Kinetics* (Ed. by A.W. Hoffmann, B. J. Giletti, H. S. Yoder & R. A. Yund), *Carnegie Institution of Washington Publication*, **634**, 205–218.

CHAI, B.H.T. (1975) *The kinetics and mass transfer of calcite during hydrothermal recrystallization process*. PhD thesis, Yale University, New Haven, CT, 138 pp.

COLBECK, S.C. (1986) Statistics of coarsening in water-saturated snow. *Acta Metall.*, **34**, 347–352.

COLBECK, S.C. (1987) Theory of particle coarsening with a log-normal distribution. *Acta Metall.*, **35**, 1583–1588.

CRAIG, H. (1957) Isotopic standards for carbon and oxygen and correction factors for mass spectrometric analysis of carbon dioxide. *Geochim. Cosmochim. Acta*, **12**, 133–149.

EBANKS, W.J. (1975) Holocene carbonate sedimentation and diagenesis, Ambergris Cay, Belize. In: *Carbonate Sediments, Clastic Sediments, and Ecology* (Ed. by K.F. Wantland & W.C. Pusey), *Am. Ass. petrol. Geol. Studies in Geology*, **2**, 234–296.

EBERL, D.D., SRODON, J., KRALIK, M., TAYLOR, B.E. & PETERMAN, Z.E. (1990) Ostwald ripening of clays and metamorphic minerals. *Science*, **248**, 474–477.

EXNER, H.E. & LUKAS, H.L. (1971) The experimental verification of the stationary Wagner-Lifshitz distribution of coarse particles. *Metallography*, **4**, 325–338.

FAIRCHILD, I.J. (1983) Effects of glacial transport and neomorphism on Precambrian dolomite crystal sizes. *Nature*, **304**, 714–716.

FAIRCHILD, I.J., HAMBREY, M.J., SPIRO, B. & JEFFERSON, T.H. (1989) Late Proterozoic glacial carbonates in northeast Spitsbergen: new insights into the carbonate–tillite association. *Geol. Mag.*, **126**, 469–490.

FAIRCHILD, I.J. & SPIRO, B. (1990) Carbonate minerals in glacial sediments: geochemical clues to paleoenvironment. In: *Glacimarine Environments: Processes and Sediments* (Ed. by J. A. Dowdeswell & J. D. Scourse), *Spec. publs geol. Soc.*, **53**, 201–216.

FOLK, R.L. (1965) Some aspects of recrystallization in ancient limestones. In: *Dolomitization and Limestone Diagenesis* (Ed. by L. C. Pray & R. C. Murray), *Spec. publs Soc. econ. Paleont. Miner.*, **13**, 14–48.

FOLK, R.L. & LAND, L.S. (1975) Mg/Ca ratio and salinity: two controls over crystallization of dolomite. *Am. Ass. petrol. Geol.*, **56**, 434–453.

FRITZ, P. & KATZ, A. (1972) The sodium distribution of dolomite crystals. *Chem. Geol.*, **10**, 237–244.

GEBELEIN, C.D., STEINEN, R.P., GARRETT, P., HOFFMAN, E.J., QUEEN, J.M. & PLUMMER, L.N. (1980) Subsurface dolomitization beneath the tidal flats of central west Andros Island, Bahamas. In: *Concepts and Models of Dolomitization* (Ed by D. H. Zenger, J. B. Dunham & R. L. Ethington), *Spec. publs Soc. econ. Paleont. Miner.*, **28**, 31–49.

GREGG, J.M. & SHELTON, K.L. (1990) Dolomitization and dolomite neomorphism in the back reef facies of the Bonneterre and Davis Formations (Cambrian), southeast Missouri. *J. sedim. Petrol.*, **60**, 549–562.

GREGG, J.M. & SIBLEY, D.F. (1984) Epigenetic dolomitization and the origin of xenotopic dolomite texture. *J. sedim. Petrol.*, **54**, 908–931.

GUNATILAKA, A., SALEH, A., AL-TEMEEMI, A. & NASSAR, N. (1987) Calcium poor dolomite from the sabkhas of Kuwait. *Sedimentology*, **34**, 999–1006.

HOHMANN, H.H. & KAHLWEIT, M. (1972) Ostwald ripening of crystalline precipitates in aqueous solutions at constant temperature and periodic temperature changes. *Ber. Bunsen Ges. phys. Chem.*, **76**, 933–938.

HOWARD, S.A. & PRESTON, K.D. (1989) Profile fitting of powder diffraction patterns. In: *Modern Powder Diffraction: Mineralogical Society of America, Reviews in Mineralogy*, Vol. 20 (Ed. by D. L. Bish & J. E. Post), pp. 217–275.

HUDSON, J.D. (1977) Stable isotopes and limestone lithification. *J. geol. Soc. London*, **133**, 637–660.

ILLING, L.V., WELLS, A.J. & TAYLOR, J.C.M. (1965) Penecontemporary dolomite in the Persian Gulf. In: *Dolomitization and Limestone Diagenesis* (Ed. by L. C. Pray & R.C. Murray), *Spec. publs Soc. econ. Paleont. Miner.*, **13**, 89–111.

JAHREN, J.S. (1991) Evidence of Ostwald ripening related recrystallization of diagenetic chlorites from reservoir rocks offshore Norway. *Clay Miner.*, **26**, 169–178.

KAUFMAN, J., HANSON, G.N. & MEYERS, W.J. (1991) Dolomitization of the Devonian Swan Hills Formation, Rosevear Field, Alberta, Canada. *Sedimentology*, **38**, 41–66.

KITANO, Y., KANAMORI, N. & OOMARI, T. (1971) Measurement of distribution coefficients of strontium and barium between carbonate precipitate and solution—abnormally high values of distribution coefficients at early stages of carbonate formation. *Geochem. J.*, **4**, 183–206.

KUPECZ, J.A. & LAND, L.S. (1991) Late-stage dolomitization of the Lower Ordovician Ellenburger Group, west Texas. *J. sedim. Petrol.*, **61**, 551–574.

KUPECZ, J.A., MONTAÑEZ, I.P. & GAO, G. (1992) Recrystallization of dolomite with time. In: *Carbonate Microfabrics* (Ed. by R. Rezak & D. Lavoie). Springer-Verlag, New York (in press).

LAND, L.S. (1980) The isotopic and trace element geochemistry of dolomite: the state of the art. In: *Concepts and Models of Dolomitization* (Ed. by D. H. Zenger, J.B. Dunham & R. L. Ethington), *Spec. publs Soc. econ. Paleont. Miner.*, **28**, 87–110.

LAND, L.S., SALEM, M.R.I. & MORROW, D.W. (1975) Paleohydrology of ancient dolomites: geochemical evidence. *Bull. Am. Ass. petrol. Geol.*, **59**, 1602–1625.

LERMAN, A. (1979) *Geochemical Processes: Water and Sediment Environments*. Wiley Interscience, New York, 481 pp.

LIFSHITZ, I.M. & SLYOZOV, V.V. (1961) The kinetics of precipitation from supersaturated solid solutions. *Physics Chem. Solids*, **19**, 35–50.

LUMSDEN, D.N. (1979) Discrepancy between thin-section and X-ray estimates of dolomite in limestone. *J. sedim. Petrol.*, **49**, 429–436.

LUMSDEN, D.N. & CHIMAHUSKY, J.S. (1980) Relationship between dolomite nonstoichiometry and carbonate facies parameters. In: *Concepts and Models of Dolomitization* (Ed. by D. H. Zenger, J. B. Dunham & R. L. Ethington), *Spec. publs Soc. econ. Paleont. Miner.*, **28**, 123–137.

LUMSDEN, D.N. & LLOYD, R.V. (1988) An update of ESR spectroscopy studies of dolomite origin. In: *Sedimentology and Geochemistry of Dolostones* (Ed. by V. Shukla & P. A. Baker), *Spec. publs Soc. econ. Paleont. Miner.*, **42**, 3–10.

MARKWORTH, A.J. (1970) The kinetic behavior of precipitate particles under Ostwald ripening conditions. *Metallography*, **3**, 197–208.

MAZZULLO, S.J. (1992) Geochemical and neomorphic alteration of dolomite, a review. *Carbonates and Evaporites*, **7** (in press).

MAZZULLO, S.J. & REID, A.M. (1988) Sedimentary textures of recent Belizean peritidal dolomite. *J. sedim. Petrol.*, **58**, 479–488.

MAZZULLO, S.J., REID, A.M. & GREGG, J.M. (1987) Dolomitization of Holocene supratidal deposits, Ambergris Cay, Belize. *Bull. geol. Soc. Am.*, **98**, 224–231.

MCKENZIE, J.A. (1981) Holocene dolomitization of calcium carbonate sediments from coastal sabkhas of Abu Dhabi, U.A.E: A stable isotope study. *J. Geol.*, **89**, 185–198.

MORSE, J.W. & CASEY, W.H. (1988) Ostwald processes and mineral paragenesis in sediments. *Am. J. Sci.*, **288**, 537–560.

ORKITA, P.M., MAYNARD, J.B., SPIKER, E.C. & FORCE, E.R. (1988) Isotopic evidence for organic matter oxidation by manganese reduction in the formation of stratiform manganese carbonate ore. *Geochim. Cosmochim. Acta*, **52**, 2679–2685.

OSTWALD, W. (1900) Über die vermeintliche Isomerie des roten und gelben Quecksilberoxyds und die Oberflächenspannung fester Körper. *Z. phys. Chem.*, **34**, 495–503.

POLGÁRI, M., OKITA, P.M. & HEIN, J.R. (1991) Stable isotope evidence for the origin of the Urkut manganese ore deposit, Hungary. *J. sedim. Petrol.*, **61**, 384–393.

POST, J.E. & BISH, D.L. (1989) Rietveld refinement of crystal structures using powder diffraction data. In: *Modern Powder Diffraction: Mineralogical Society of America, Reviews in Mineralogy*, Vol. 20 (Ed. by D. L. Bish & J. E. Post), pp. 277–308.

REEDER, R.J. (1981) Electron optical investigation of sedimentary dolomites. *Contr. Miner. Petrol.*, **76**, 148–157.

RIETVELD, H.M. (1969) A profile refinement method for nuclear and magnetic structures. *J. appl. Crystallogr.*, **2**, 65–71.

SASS, E. & BEIN, A. (1988) Dolomites and salinity: a comparative geochemical study. In: *Sedimentology and Geochemistry of Dolostones* (Ed. by V. Shukla & P.A. Baker), *Spec. publs Soc. econ. Paleont. Miner.*, **43**, 223–233.

SHINN, E.A., GINSBURGH, R.N. & LLOYD, R.M. (1965) Recent supratidal dolomite from Andros Island, Bahamas. In: *Dolomitization and Limestone Diagenesis* (Ed. by L. C. Pray & R. C. Murray), *Spec. publs Soc. Paleont. Miner.*, **13**, 112–123.

SIBLEY, D.F. & GREGG, J.M. (1987) Classification of dolomite rock textures. *J. sedim. Petrol.*, **57**, 967–975.

SIBLEY, D.F., GREGG, J.M., BROWN, R.G. & LAUDON, P.R. (1992) Dolomite crystal size distribution. In: *Carbonate Microfabrics* (Ed. by R. Rezak & D. Lavoie). Springer-Verlag, New York (in press).

STEEFEL, C.I. & VAN CAPPELLEN, P. (1990) A new kinetic approach to modeling water–rock interaction: the role of nucleation, precursors, and Ostwald ripening. *Geochim. Cosmochim. Acta*, **54**, 2657–2677.

VAHRENKAMP, V.C. & SWART, P.K. (1990) New distribution coefficient for the incorporation of strontium into dolomite and its implications for the formation of ancient dolomites. *Geology*, **18**, 387–391.

WAGNER, C. (1961) Theorie der Alterung von Niederschlägen durch Umlösen (Ostwald Reifung). *Z. Elektrochem.*, **65**, 581–591.

WALTON, A.G. (1969) Nucleation in liquids and solutions. In: *Nucleation* (Ed. by A. C. Zettlemoyer), pp. 225–307. Marcel Dekker, New York.

ZENGER, D.H. & DUNHAM, J.B. (1988) Dolomitization of Siluro-Devonian limestones in a deep core (5350 M) southeastern New Mexico. In: *Sedimentology and Geochemistry of Dolostones* (Ed. by V. Shukla & P. A. Baker), *Spec. publs Soc. econ. Paleont. Miner.*, **43**, 160–173.

(Manuscript received 26 June 1991; revision received 3 October 1991)